JACS
JOURNAL OF THE AMERICAN CHEMICAL SOCIETY
pubs.acs.org/JACS
Article

Regiochemistry-Driven Organic Electrochemical Transistor Performance Enhancement in Ethylene Glycol-Functionalized Polythiophenes

Rawad K. Hallani, Bryan D. Paulsen, Anthony J. Petty II, Rajendar Sheelamanthula, Maximilian Moser, Karl J. Thorley, Wonil Sohn, Reem B. Rashid, Achilleas Savva, Stefania Moro, Joseph P. Parker, Oscar Drury, Maryam Alsufyani, Marios Neophytou, Jan Kosco, Sahika Inal, Giovanni Costantini, Jonathan Rivnay, and Iain McCulloch*

Cite This: J. Am. Chem. Soc. 2021, 143, 11007−11018

ABSTRACT: Novel p-type semiconducting polymers that can facilitate ion penetration, and operate in accumulation mode are much desired in bioelectronics. Glycol side chains have proven to be an efficient method to increase bulk electrochemical doping and optimize aqueous swelling. One early polymer which exemplifies these design approaches was p(g2T-TT), employing a bithiophene-*co*-thienothiophene backbone with glycol side chains in the 3,3′ positions of the bithiophene repeat unit. In this paper, the analogous regioisomeric polymer, namely pgBTTT, was synthesized by relocating the glycol side chains position on the bithiophene unit of p(g2T-TT) from the 3,3′ to the 4,4′ positions and compared with the original p(g2T-TT). By changing the regiopositioning of the side chains, the planarizing effects of the S−O interactions were redistributed along the backbone, and the influence on the polymer's microstructure organization was investigated using grazing-incidence wide-angle X-ray scattering (GIWAXS) measurements. The newly designed pgBTTT exhibited lower backbone disorder, closer π-stacking, and higher scattering intensity in both the in-plane and out-of-plane GIWAXS measurements. The effect of the improved planarity of pgBTTT manifested as higher hole mobility (μ) of 3.44 ± 0.13 cm^2 V^{-1} s^{-1}. Scanning tunneling microscopy (STM) was in agreement with the GIWAXS measurements and demonstrated, for the first time, that glycol side chains can also facilitate intermolecular interdigitation analogous to that of pBTTT. Electrochemical quartz crystal microbalance with dissipation of energy (eQCM-D) measurements revealed that pgBTTT maintains a more rigid structure than p(g2T-TT) during doping, minimizing molecular packing disruption and maintaining higher hole mobility in operation mode.

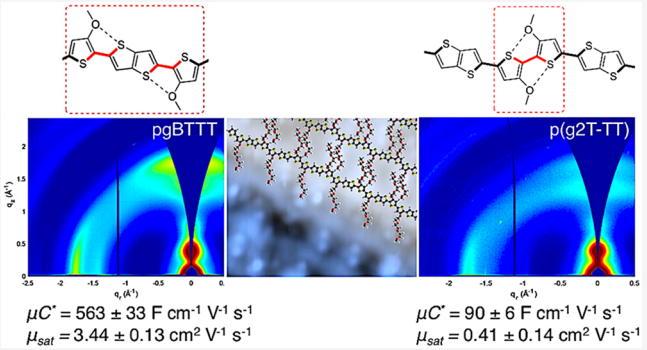

INTRODUCTION

Bioelectronics is an interdisciplinary field that involves the fabrication of electronic devices capable of communicating with biological systems by translating biological signals (e.g., ion fluxes), into electronic signals. In the past decade, the field has seen significant growth in the number of device types employed, and applications thereof, including polymer electrodes for neural interfacing,[1] organic electrochemical ion pumps for drug delivery systems,[2,3] and organic electrochemical transistors (OECTs) for the signal amplification of ionic fluxes and sensing of molecules and ions,[4,5] as well as many others.[6−8] Each of these applications relies on the use of semiconducting materials that exhibits "mixed" transport,[9] i.e., materials that can transport both ionic and electronic charge carriers.[10] Conjugated organic polymeric materials possess weak intermolecular (van der Waals) interactions, which allow ionic diffusion within the microstructure, making this type of materials ideal for biological applications.[11] At the same time, conjugated polymers are well-known for exhibiting excellent electronic charge carrier characteristics and have exceptional synthetic flexibility,[12,13] and are thus ideal candidates for creating communication across the abiotic/biotic interface.

From the many bioelectronic devices developed, OECTs have gained significant interest in the past decade.[14] In contrast to organic field-effect transistors (OFETs), OECTs use (often aqueous) electrolytes as gate dielectrics, with subsequent ion-charge transport throughout the bulk of the thin film.[10] Given

Received: April 2, 2021
Published: June 30, 2021

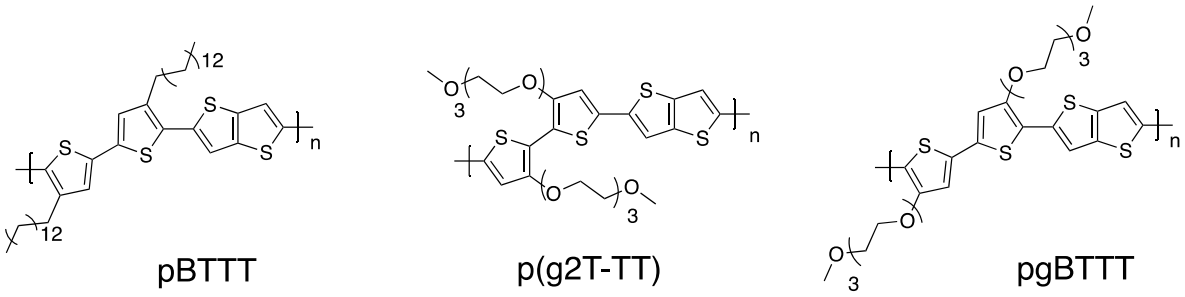

Figure 1. pBTTT, p(g2T-TT), and pgBTTT polymer structures.

the predominant use of OECTs to monitor biosignals, the electrolyte solution in contact with an OECT channel is typically one that mimics biological conditions, e.g., an aqueous 100 mM NaCl solution.[15] For OECTs to operate efficiently, the organic semiconductor in the channel must allow ion transport throughout the bulk of the film enabled upon applying a bias at the gate electrode.[14] As ions coordinate to water molecules, ion motion into the organic semiconductor is typically accompanied by an ingress of water molecules into the semiconductor as well, thereby leading to a swelling of the polymer.[16,17] The coupling of these ions with the electronic charges in the polymer backbone affects the channel conductivity, and hence is transduced as an electrical signal.[17]

Currently, the most widely employed channel material in OECTs is the polyelectrolyte doped conducting polymer poly(3,4-ethylene dioxythiophene)-poly(styrenesulfonate) (PEDOT:PSS). PEDOT:PSS has been heavily studied as the active semiconducting material in OECTs because of its electrical conductivity of >1000 S cm^{-1}, commercial availability from many suppliers, and electrochemical stability.[18,19] Nonetheless, PEDOT:PSS-based OECTs display some drawbacks, including the requirement of a depletion mode of operation (due to its intrinsic conductivity) that increases the power consumption of the device, meaning that PEDOT:PSS-based devices are typically ON in the absence of gate bias. Once a positive bias is applied, cations are injected into the channel and de-dope PEDOT:PSS, thereby modulating its electrical conductivity and the drain current recorded. Additionally, the complex structure of PEDOT:PSS limits its use as a model system to investigate structure−property relations.[20] Moreover, the PSS fraction in PEDOT:PSS acts as an electrical insulator and limits the volumetric capacitance (C*).[21] Added to that, PEDOT:PSS requires extensive pre- and postprocessing treatments to achieve optimum performance in OECT applications.[22] To overcome the limitations posed by PEDOT:PSS, the last five years have witnessed the development of a new class of organic semiconducting polymers employing electron rich thiophene backbones grafted with ethylene glycol (EG)-based side chains, whose electronic, morphological and swelling properties can be easily tailored by chemical design.[14,23−26] These materials have shown considerable promise for bioelectronic applications as (i) their OECT performance can match or even exceed those of PEDOT:PSS-based devices,[23,27] (ii) OECTs employing these materials typically operate in accumulation mode compatible with conventional circuits,[23,28] and (iii) they are ideal materials for biosensing due to the flexibility of customized side chains that offer a wide tunability of the surface properties.[16,29−31]

Previous work has demonstrated the ability to manipulate conjugated polymers through molecular design in order to enhance their ionic and electronic conductivities by (i) improving orbital interchain overlapping for better intermolecular charge transport, (ii) increasing π-conjugation for intramolecular charge delocalization, (iii) tuning energy levels (the highest occupied molecular orbital, HOMO, for p-type polymers and the lowest unoccupied molecular orbital, LUMO, for n-type polymers),[32−34] and (iv) introducing glycol chains to improve ion doping efficiency and aqueous compatibility.[17,23,28,35,36] So far, the molecular design strategies investigated to maximize the OECT performance of EG functionalized organic semiconductors have been focused either on tuning the nature and length of the employed side chains or modifying the aromatic moieties that constitute the conjugated polymer backbone.[16,17,23,27,28,30,31,35,36] Of the numerous EG-functionalized organic semiconductors developed for OECT applications, poly(2-(3,3′-bis(2-(2-(2-methoxyethoxy)ethoxy)ethoxy)-[2,2′-bithiophen]-5-yl)thieno-[3,2-*b*]thiophene) (p(g2T-TT)), a polymer whose conjugated backbone consists of alternating 3,3′-diglycoxy-2,2′-bithiophene and thienothiophene units, has been demonstrated to be one of the highest performing active channel materials for OECTs, affording a μC* figure of merit up to 261 F cm^{-1} V^{-1} s^{-1}.[37] p(g2T-TT)'s high performance in OECTs has been attributed both to its high volumetric capacitance, which is a result of the polymer's ability to accept ions extensively throughout the bulk, and its good electronic mobility (μ_{OECT}), which stems from the relatively high degree of polymer backbone planarity that arises due to the planarizing sulfur−oxygen interactions of the head-to-head coupled bithiophene moiety.[23] Close examination of the p(g2T-TT) backbone reveals that the side chains have an isomeric regio-arrangement to the well-known semiconducting polymer pBTTT, shown in Figure 1, where in this case, the side chains have a head-to-head regiopositioning. The side chains of p(g2T-TT) have an oxygen atom directly connected to the thiophene repeat unit, which increases both backbone planarization and electron density. The regio-positioning of the oxygen atom therefore is likely to have direct consequences on both parameters.

Herein, we investigate the regiochemical attachment of the solubilizing triethylene glycol (TEG) chains on the 2,2′-bithiophene unit at the 4,4′-positions (tail-to-tail linkage) in comparison to the 3,3′-positions (head-to-head linkage) in the analogous polymer p(g2T-TT) (see Figure 1) and discuss the origins of the difference in materials properties. Density functional theory (DFT) simulations predict that the resulting polymer, poly(2-(4,4′-bis(2-methoxyethoxy)-5′-methyl-[2,2′-bithiophen]-5-yl)-5-methylthieno[3,2-b]thiophene) (pgBTTT), should have an increased ratio of planar dihedral angles across the backbone (*vide infra*), which should improve the backbone planarity, reducing energetic disorder, and

https://doi.org/10.1021/jacs.1c03516
J. Am. Chem. Soc. 2021, 143, 11007−11018

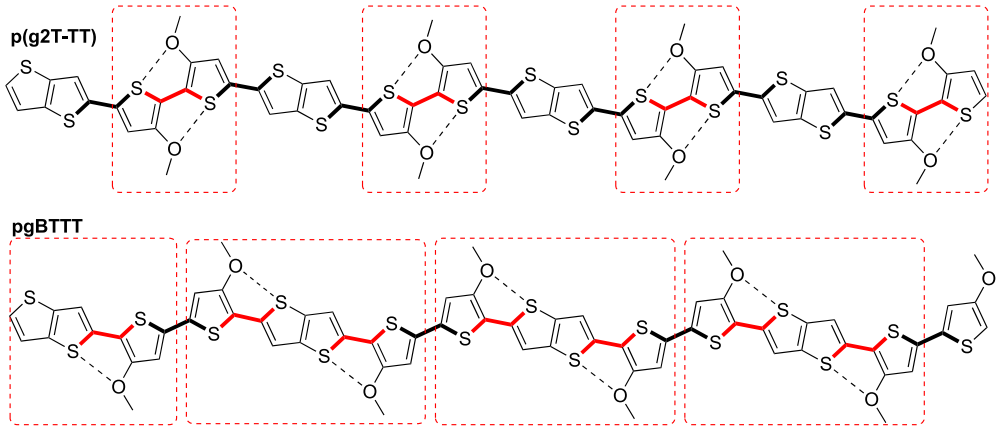

Figure 2. Sections of p(g2T-TT) and pgBTTT polymers highlighting S−O interactions (black dashed lines) leading to planarized dihedrals (bold red with θ = 177−180°), and sections with twisted dihedrals in the absence of the S−O interactions (bold black with θ = 154−156°). The red dashed squares highlight the planar sections in pgBTTT and p(g2T-TT). Geometries were optimized using ωB97XD/6-31G* where ω = 0.1 Bohr^{-1}.

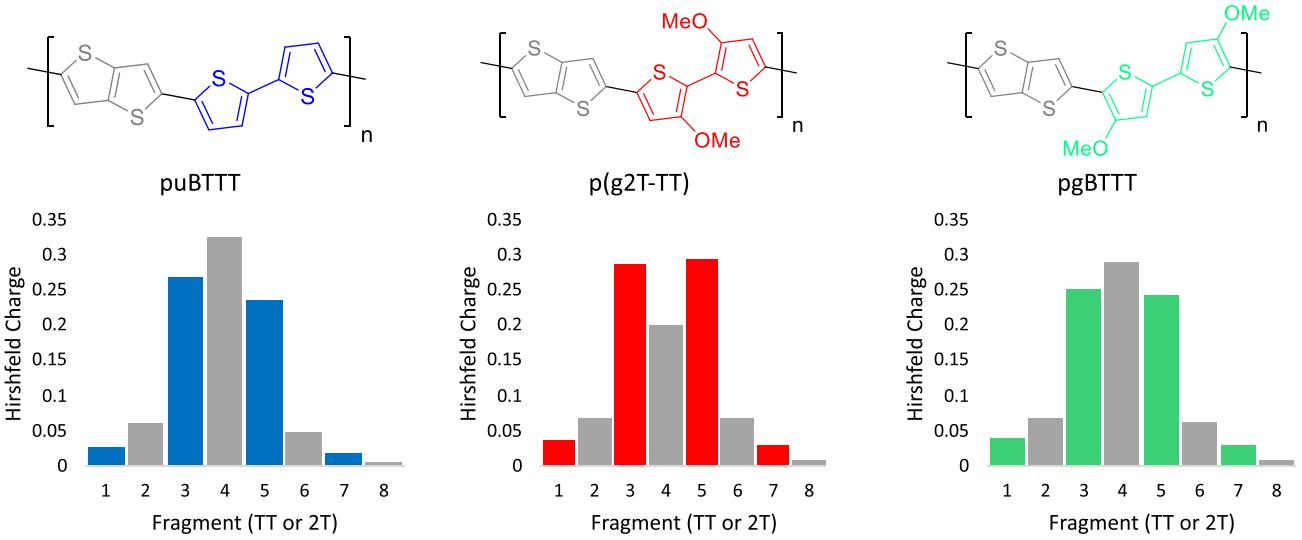

Figure 3. Hirshfeld charge distribution in oxidized puBTTT, p(g2T-TT), and pgBTTT polymers based on a fragment analysis of the polymer chain. TT groups shown in gray, 2T or dimethoxy-2T groups shown in other colors. All optimizations and charge analysis were performed with ωB97XD/6-31G*.

therefore improving the polymer's charge carrier mobility. Monomethyl ether-capped TEG chains were employed as solubilizing units as previous investigations into polythiophene-based polymers for OECT applications had revealed that these chains facilitate a good compromise for both μ_{OECT} and C^*.[36] Moreover, the use of TEG chains also allowed for a more direct and fairer comparison of the resulting polymer with p(g2T-TT).[23,28] A detailed comparison between the two isomeric polymers was made using photoelectron spectroscopy in air (PESA), cyclic voltammetry (CV), spectroelectrochemistry, UV−vis absorption spectroscopy, differential scanning calorimetry (DSC), grazing incidence wide-angle X-ray scattering (GIWAXS) and scanning tunneling microcopy (STM), in order to have a full understanding of the polymers' physical, structural, and electronic properties. Compared to p(g2T-TT), OECTs fabricated from pgBTTT showed a much-improved mobility, leading to a record high average μC^* of 502 ± 18 F cm^{-1} V^{-1} s^{-1}.

EXPERIMENTAL SECTION

Theoretical Modeling. To examine the effect of the intramolecular S−O interactions on the conformation of the backbone, oligomers of pgBTTT and p(g2T-TT) were modeled by DFT simulations, where TEG chains were truncated to OMe groups for computational efficiency. From the 4-oligomers' illustration in Figure 2 it can be seen that some of the dihedral angles become stabilized by noncovalent S−O interactions resulting in four dihedral angles close to 180° in p(g2T-TT). In contrast, seven dihedrals were close to 180° in a pgBTTT oligomer of the same length, showing a higher degree of regularity in dihedral angles across the backbone of pgBTTT (Figure 2). This reduced fluctuation in dihedral angles is evidence of a more planar backbone, allowing closer intermolecular π−π distances and reducing energetic disorder, which should in turn facilitate charge hopping, and therefore enhance charge carrier mobilities.[38] The S−O interactions in p(g2T-TT) are additive, as torsional potential energy surfaces (see Supporting Information) show the largest barrier for rotation, and therefore more stabilization at the planarized minima, for p(g2T-TT) around the thiophene−thiophene bond.

Ionization potential levels can be affected by both geometric and electronic effects which can be investigated separately using model systems. In order to analyze the relevance of the geometric effects, the

https://doi.org/10.1021/jacs.1c03516
J. Am. Chem. Soc. 2021, 143, 11007−11018

alkoxy groups of both polymers' backbones were removed, forming an equivalent unsubstituted bithiophene-*co*-thienothiophene model polymer puBTTT. The HOMO level was estimated by calculation of the oxidation potential in a polarizable continuum, with the fully optimized unsubstituted polymer puBTTT having a HOMO energy of −5.34 eV with respect to the vacuum level. Using the p(g2T-TT) derived geometry with the methoxy groups replaced with protons, results in the HOMO being shallower by 0.1 to −5.2 eV. The pgBTTT derived geometry with methoxy groups replaced by protons gave a HOMO energy of −5.1 eV, as a result of the substantial increase in the quantity of planar dihedral angles throughout the pgBTTT backbone.

Generally, reducing torsional disorder in the polymers' backbone leads to an improvement in charge carrier mobilities.[38] However, charge distribution within the polymer could also have a substantial effect on charge mobilities. To quantify the charge distribution effect, the polymers were divided into fragments, and the Hirshfeld charges of each fragment along the polymer chain were calculated (Figure 3). The charge distribution in pgBTTT is very similar to the puBTTT polymer, with one-third of the overall charge of the oxidized polymers residing on a TT group near the middle of the system. In contrast, the charge in p(g2T-TT) is more stabilized on the bithiophene units than on the TT. Thus, the HOMO energy of p(g2T-TT) is raised more than that of pgBTTT by the electron donation effects, due to the proximity of OMe substituents to the positive charge. These are purely electronic effects and not induced by the polymer conformation, as charge distributions of unsubstituted polymer chains with dihedrals fixed at the pgBTTT or p(g2T-TT) geometries resemble that of parent puBTTT (see Figure S7). Overall, HOMO levels of both p(g2T-TT) and pgBTTT are shallower relative to puBTTT through both geometric and electronic effects, although the geometric effect is stronger in pgBTTT while the electronic effect is stronger in p(g2T-TT).

Material Synthesis and Characterization. Although pgBTTT has a very similar chromophore to that of p(g2T-TT), the synthesis of this polymer has proven to be quite challenging. The homocoupling step of the thiophenes to generate the bithiophene monomer had to be done via a CH homocoupling reaction to obtain the correct regio isomeric monomer, while the purification of that monomer was unexpectedly challenging. The synthesis of pgBTTT commenced with the transetherification of 3-methoxy-thiophene with triethylene glycol monomethyl ether in toluene using *p*-toluene sulfonic acid as a catalyst to form 3-(triethylene glycol monomethyl ether)thiophene (**2**) in 60% yield. 3-(Triethylene glycol monomethyl ether)thiophene (**2**) was subsequently brominated with *N*-bromosuccinimide in tetrahydrofuran to generate 2-bromo-3-(triethylene glycol monomethyl ether)thiophene (**3**). A C−H homocoupling reaction of 2-bromo-3-(triethylene glycol monomethyl ether)thiophene (**3**) using silver nitrate, potassium fluoride and $PdCl_2(PhCN)_2$ as the catalyst was employed to produce 5,5′-dibromo-4,4′-bis(triethylene glycol monomethyl ether)-2,2′-bithiophene (**4**) in 55% yield.[39] Finally, polymerization of 5,5′-dibromo-4,4′-bis(triethylene glycol monomethyl ether)-2,2′-bithiophene (**4**) with 2,5-bis(trimethyl stannyl)-thieno[3,2-*b*]thiophene was performed in a microwave setup using $Pd_2(dba)_3$ as the catalyst and P(*o*-tol)$_3$ as the ligand to afford pgBTTT with an M_n of 10 kDa and an M_w of 24 kDa.

The reference p(g2T-TT) polymer was synthesized following a previously reported literature procedure.[17] p(g2T-TT) was obtained with an M_n of 7 kDa and an M_w of 20 kDa, comparable to those of pgBTTT, thus allowing for a fair comparison between the two polymers.

UV−vis spectroscopy was carried out on polymer films while applying a −0.3 V bias to ensure that each polymer was in its fully discharged state. As can be seen from Figure S15, changing the regiochemistry of the solubilizing EG side chains on the conjugated polymer backbone did not have a significant impact on the optical properties, with pgBTTT and p(g2T-TT) exhibiting a maximum wavelength $\lambda_{max,film}$ (wavelength at which the polymer has its strongest photon absorption) of 596 and 597 nm and an optical band gap $E_{g,opt}$ of 1.73 and 1.74 eV, respectively. The main absorption feature in both polymers was ascribed to a $\pi-\pi^*$ optical transition. Both polymers also featured a low energy shoulder around 650 nm, which was attributed to a 0−0 vibronic transition. This 0−0 vibronic transition was better resolved in pgBTTT than p(g2T-TT), hence suggesting increased ordering in the solid state in pgBTTT compared to p(g2T-TT), which is in agreement with the reduced torsional disorder of the pgBTTT backbone as demonstrated with the DFT calculations and is further confirmed by GIWAXS measurements (*vide infra*).

The polymers' electrochemical properties were evaluated through a combination of techniques, including PESA, UV−vis spectroscopy, and CV, see Supporting Information for details concerning the experimental setup and sample preparation. The polymers' optical and electronic properties, including their onset of oxidation in organic media ($E_{ox,org}$), aqueous media ($E_{ox,aq}$), IPs (measured using PESA), maximum absorption wavelength in the solid state ($\lambda_{max,film}$) and optical gap ($E_{g,opt}$) are summarized in Table 1. The IP of pgBTTT was estimated to be 4.73 eV compared to p(g2T-TT) IP of 4.55 eV. As the thin films are exposed to an aqueous 100 mM NaCl electrolyte solution in operation, measuring the IP of these polymers with cyclic voltammetry should give a more explicit description of the expected IPs, as thin-film CV can be performed in aqueous electrolyte and organic electrolyte environments. The cyclic voltammograms recorded for pgBTTT and p(g2T-TT) are shown in Figure S17. Both polymers can be doped reversibly employing both an aqueous and an organic supporting electrolyte. The IP of pgBTTT with CV in organic electrolytes ($TBAPF_6$ in acetonitrile) was measured to be 4.63 eV, similar to p(g2T-TT)'s IP of 4.61 eV. However, pgBTTT thin films exhibited a shift in the onset of oxidation in both organic (from −0.09 to −0.07 V vs Ag/AgCl) and aqueous media (from −0.14 to −0.04 V vs Ag/AgCl) to more positive potentials, whereby a more pronounced shift was observed when employing an aqueous electrolyte.

Table 1. Summary of the Optical and Electronic Properties of the Polymers under Investigation

polymer	$E_{ox,org}$[a] (V)	$E_{ox,aq}$[b] (V)	IP[c] (eV)	IP[d] (eV)	$\lambda_{max,film}$[a] (nm)	$E_{g,opt}$[e,f] (eV)
pgBTTT	−0.07	−0.04	4.63	4.73	596	1.73
p(g2T-TT)	−0.09	−0.14	4.61	4.55	597	1.74

[a]Determined employing a 0.1 M tetrabutylammonium hexafluorophosphate in acetonitrile solution. [b]0.1 M sodium chloride in deionized water solution as the supporting electrolyte. [c]Calculated from IP (eV) = ($E_{ox,org}$ − E_{Fc} + 5.1), where E_{Fc} is the half-wave potential of the ferrocene/ferrocenium (Fc/Fc^+) redox couple. [d]Determined using photoelectron spectroscopy in air. [e]Value obtained while applying a potential of −0.3 V vs an Ag/AgCl reference electrode. [f]Determined from the onset of absorption.

Spectroelectrochemistry was employed to gain insights into the doping mechanism of the polymers. As can be seen from Figures S15 and S16, no significant differences were observed in the recorded spectroelectrochemistry data when conducting the measurements in an aqueous or organic electrolyte. Figures S15 and S16 show that both pgBTTT and p(g2T-TT) were doped under ambient conditions, thus requiring the application of a negative bias (−0.3 V) to fully de-dope the polymers. As already suggested by the CV data, the larger IP of pgBTTT resulted in a lower extent of doping under ambient conditions compared to p(g2T-TT), thus explaining the slightly higher normalized absorbance of its $\pi-\pi^*$ transition under 0.0 V compared to p(g2T-TT). Progressive increments in the applied bias up to +0.5 V vs Ag/AgCl resulted in a gradual depression of the pgBTTT and p(g2T-TT) $\pi-\pi^*$ transitions with a concomitant appearance of a lower energy absorption band around 900 nm, which was ascribed to the formation of the polymers' polaronic species. Further increasing the applied bias to +0.8 V resulted in the depression of this more extended absorption feature. In parallel, a new, lower energy absorption feature emerged around 1110 nm, which was related to the formation of polaronic/bipolaronic forms of

https://doi.org/10.1021/jacs.1c03516
J. Am. Chem. Soc. 2021, 143, 11007−11018

the polymers. To test the reversibility of the doping process, the applied potential was reversed to −0.5 V. The complete restoration of the optical signature of the fully de-doped polymer species of the two polymers under investigation suggests that both polymers can be discharged stably and reversibly in both aqueous and organic media without showing any significant signs of degradation in the specified potential window.

RESULTS AND DISCUSSION

Microstructure. GIWAXS was carried out to investigate the structural effects of oligoethylene glycol side chain regiopositioning. Both pgBTTT and p(g2T-TT) films display an oriented microstructure(more so than their unannealed alkylated counterpart),[40] with two orders of scattering from in-plane π-stacked lamella, (h00), occurring out of plane and a corresponding lamellar spacing of 16.5 and 15.5 Å for pgBTTT and p(g2T-TT), respectively (see Table 2). Faint first order in-plane lamellar scattering was observed in pgBTTT but was completely absent in p(g2T-TT) (see Figure 4). Scattering from π-stacking, (010), was not isotropic but shows pronounced intensity in- and out-of-plane for both polymers, indicating a mix of edge-on and face-on crystallites. In the case of pgBTTT, (010) peak intensity was stronger than p(g2T-TT), especially out-of-plane. This suggests that pgBTTT crystallites were more evenly mixed between edge-on and face-on, while p(g2T-TT) crystallites were majority edge-on. The lack of clear in-plane lamellar peaks indicates that though the face-on crystallites were ordered in the π-stacking direction, they did not have corresponding lamellar ordering. On the whole, while nominally identical thickness films were analyzed for both polymers, pgBTTT produced five times the scattering intensity as p(g2T-TT), implying a higher fraction of ordered polymers (i.e., more scattering events) in pgBTTT.

Table 2. GIWAXS Fit Peak Centers and Calculated *d*-Spacing

index		in-plane		out-of-plane	
		pgBTTT	p(g2T-TT)	pgBTTT	p(g2T-TT)
(100)	q (Å^{-1})			0.381	0.406
	d (Å)			16.5	15.5
(010)	q (Å^{-1})	1.775	1.753	1.746	1.744
	d (Å)	3.54	3.58	3.60	3.60
(001)	q (Å^{-1})	1.416	0.973		
	d (Å)	4.43	6.46		
broad mid-q peak	q (Å^{-1})			1.377	1.365
	d (Å)			4.56	4.60

The in-plane pgBTTT d-spacing in the π-stack direction, (010), was calculated to be marginally smaller than the corresponding one for p(g2T-TT), while the out-of-plane d-spacings in the π-stack direction were identical, Table 2. More conspicuously, the out-of-plane pgBTTT lamellar spacing was calculated to be 1.0 Å larger than p(g2T-TT). In addition to higher pgBTTT scattering intensity, implying a higher density of crystallites, the pgBTTT coherence lengths (L_c) of the (010) π-stack scattering peaks estimated by the Scherrer equation were 11% and 31% larger than for p(g2T-TT), in and out of plane, respectively (Table S1). This increase in the number of crystallites and coherence lengths is mirrored in improved electronic charge transport.

In-plane, pgBTTT shows a peak at 1.42 Å^{-1} while p(g2T-TT) shows a peak at 0.97 Å^{-1} both of which have been tentatively indexed as (001) (see Figure S12). The 1.42 Å^{-1} pgBTTT peak was similar to one observed in alkylated pBTTT.[41] In the alkylated case, though, this peak was indexed as (003) due to the presence of higher order peaks roughly following multiples of 0.47 Å^{-1}, relating these peaks to the estimated repeat unit length of 13.3 Å.[40] However, in the case of pgBTTT, higher order multiples are absent. Additionally, it was not immediately clear what selection rules only allow reflections of order n+2. Therefore, in the case of pgBTTT we were hesitant to ascribe this peak position to reflections arising from the repeat unit length along the direction of the polymer backbone. Interestingly, the calculated d-spacing of 4.43 Å is similar to the expected spacing between oligoethylene glycol helices.[42] Out-of-plane there existed a broad mid-q peak (∼1.4 Å^{-1}) for both polymers, also roughly consistent with the spacing between oligoethylene glycol helices.

For p(g2T-TT), the in-plane (001) peak was shifted to lower q giving a calculated d-spacing of 6.46 Å, roughly half the polymer repeat unit, which was consistent with alternating cofacial registration of the bithiophene and thienothiophene repeat units, similar to that observed in naphthalenedicarboximide bithiophene alternating copolymers.[43−45] As side chain

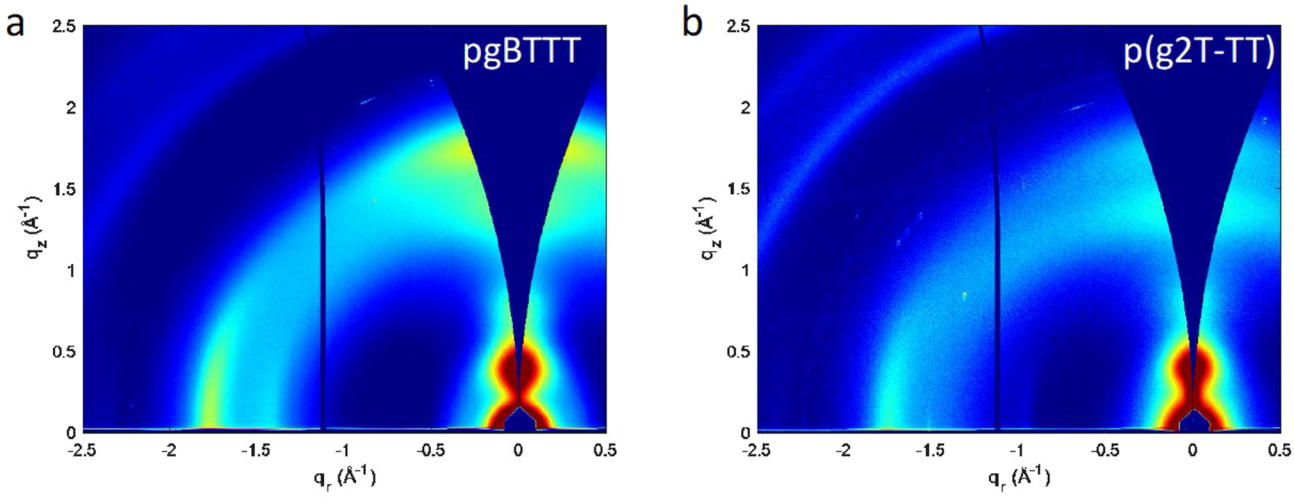

Figure 4. Two-dimensional grazing incidence X-ray q_r−q_z scattering map of (a) pgBTTT and (b) p(g2T-TT) thin films.

https://doi.org/10.1021/jacs.1c03516
J. Am. Chem. Soc. 2021, 143, 11007−11018

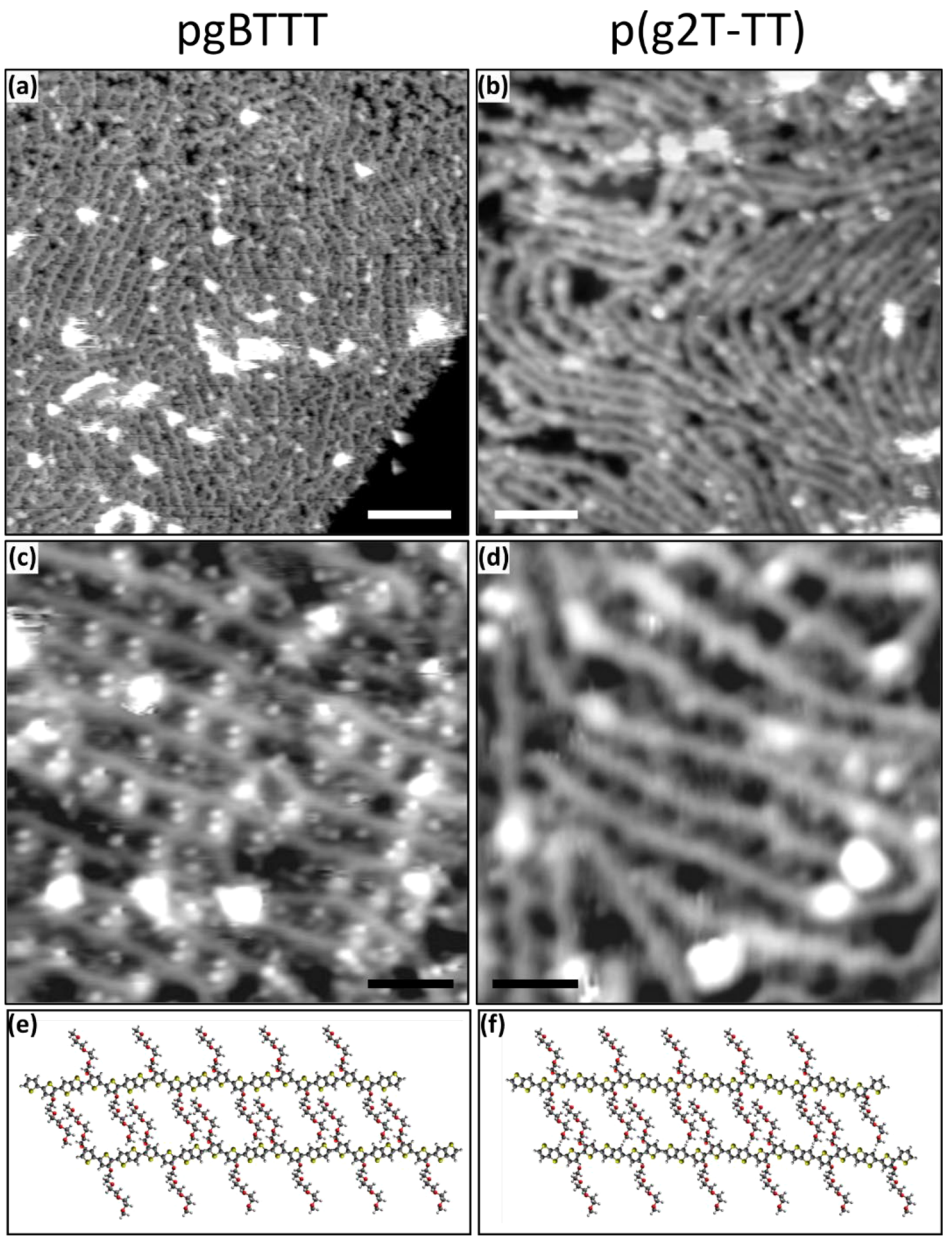

Figure 5. STM images of high coverage areas of (a) pgBTTT and (b) p(g2T-TT) deposited in vacuum by ESD on a Au(111) substrate. Smaller scale (15 × 15 nm^2) STM images for (c) pgBTTT and (d) p(g2T-TT) show locally parallel backbones separated by regularly spaced features that are ascribed to the triethylene glycol side chains. (e) and (f) show geometry-optimized molecular models of pairwise interdigitated polymers derived from the STM results for pgBTTT and p(g2T-TT), respectively. All images were acquired at −196 °C. Scale bars in (a) and (b) correspond to 10 nm, in (c) and (d) to 3 nm. Scanning parameters: (a) sample bias −1.4 V, set point current 75 pA; (b) +1.5 V, 80 pA; (c) −0.8 V, 190 pA; (d) 1.2 V, 80 pA.

placement has been previously shown to direct cofacial registration, it is plausible that the p(g2T-TT) head-to-head side-chain arrangement could force a particular cofacial registration while the pgBTTT tail-to-tail side-chain arrangement would not.

In order to get a better understanding of the intermolecular interactions and the assembly of pgBTTT and p(g2T-TT), the two polymers were transferred by electrospray deposition (ESD) onto a Au(111) surface and analyzed in ultrahigh vacuum by means of low temperature scanning tunneling microscopy (LT-STM). This technique has recently been shown to provide valuable information about the sequence, defects and microstructure of conjugated polymers.[46−49] Both polymers adsorb on the Au(111) substrate face-on, forming two-dimensional (2D) islands where individual backbones can be recognized as bright, elongated structures with occasional bends (Figure 5a,b). Although the high-degree of order reported for conjugated polymers with alkylated side chains is not achieved by either of these two glycolated polymers,[46,50,51] at high molecular coverages both polymers tend to organize into extended, compact structures with locally parallel backbones, as seen in Figure 5c,d. Measurements of the interstrand distances in these regular areas give a distribution of values of 15 ± 2 Å (average ± standard deviation) for both pgBTTT and p(g2T-TT). Since this distance is the 2D equivalent of the lamellar spacing, the fact that the STM values are compatible with the GIWAXS results (Table 2), suggests

https://doi.org/10.1021/jacs.1c03516
J. Am. Chem. Soc. 2021, 143, 11007−11018

Table 3. OECT Parameters and Material Figures of Merit

	g_m (mS)[a]	d (nm)	V_t (mV)[b]	μ_{sat} (cm^2 V^{-1} s^{-1})[b]	C* (F cm^{-3})[c]	$\mu_{sat} \times C^*$ (F cm^{-1} V^{-1} s^{-1})	μC^* (F cm^{-1} V^{-1} s^{-1})[a]
pgBTTT	21.0 ± 0.7	108 ± 1	−242.9 ± 4.9	3.44 ± 0.13	164 ± 7	563 ± 33	502 ± 18
p(g2T-TT)	6.2 ± 0.6	111 ± 10	14.7 ± 16.1	0.41 ± 0.14	244 ± 51	90 ± 6	93 ± 13

[a]Maximum transconductance and μC^* extracted from the slope of saturated transfer curves at −0.6 V. [b]Threshold voltage and saturation mobility extracted from fits of $I_d^{1/2}$ vs V_g plots. [c]Average volumetric capacitance beyond threshold voltage determined by electrochemical impedance spectroscopy. Reported uncertainties are one standard deviation, with $n = 6$ devices.

that the polymers adopt a local planar geometry also in the crystallites of 3D thin films.

Smaller scale STM images (see for example Figure 5c,d for pgBTTT and p(g2T-TT), respectively) show bright features periodically arranged in between the backbones of neighboring polymers. In the case of pgBTTT it was possible to achieve a higher resolution, revealing a series of double dots that appear on both sides of the backbones (Figure 5c). The measured separation between successive pairs of double dots on the same side of a backbone is 13.5 ± 0.5 Å, matching well with the expected pgBTTT repeat unit length (13.75 Å, see Figure S13). The separation between successive pairs of double dots on opposite sides of the backbones (6.5 ± 0.5 Å) is also consistent with the calculated distance between the 2- and 4-positions of two successive thiophenes (6.42 Å). This analysis strongly indicates that the pairs of double dots can be attributed to the triethylene glycol side chains of neighboring polymers interacting with one another, suggesting that the on-surface assembly of pgBTTT is driven by side chain interdigitation. While side chain interdigitation has been amply demonstrated for various types of alkylated polymers,[41,46,52] to the best of our knowledge, no direct evidence of interdigitation for glycol side chains has yet been reported in the literature. The interaction between the triethylene glycol side chains is expected to mimic that of crystalline oligoethylene glycol antiparallel helices,[42] thereby supporting the interpretation of the GIWAXS results for pgBTTT (*vide supra*). The analysis of the STM images further implies a pairing of the triethylene glycol chains, rather than the fully interdigitated and equispaced sequence of side chains typically observed for alkylated polymers. This arrangement is expected to be a direct consequence of the spacing between the triethylene glycol chains along the backbone (side chain attachment density), i.e. of the polymer structure itself.

Figure 5e displays a molecular model of the interaction between neighboring pgBTTT strands (individually optimized with the MMFF94s force field of the Avogadro molecular editor) that summarizes the previous observations. Scaled versions of this model show a good agreement with the STM images, with both backbones and side-chains being well described (see Figure S14). An analogous model is shown for p(g2T-TT) in Figure 5f. While it was not possible to directly derive this model from the analysis of the STM data acquired for p(g2T-TT) (because of their lower resolution), its superposition on scaled images displays a good agreement with all the visible features (see Figure S14). Finally, it should be noted that the interaction of the polymers' backbones with the Au(111) surface will have a significant planarizing effect on their conformation, likely to be stronger than the calculated torsional energy barriers. As a consequence, we do not expect the STM measurements to reveal any major difference in the backbone conformation suggested by the DFT calculations.

Although a well-ordered interdigitation (as observed by STM) cannot be conclusively deduced from the GIWAXS patterns collected, since it would require GIWAXS patterns with multiple orders of mixed index peaks that allow enough scattering features to model the unit cell, the GIWAXS measurements do report a (100) d-spacing of 16.5 and 15.5 Å for pgBTTT and p(g2T-TT), respectively (see Table 2). On the other hand, the STM measurements report a distance between the interdigitated polymers of 15 ± 2 Å (measured perpendicularly from backbone to backbone) for both pgBTTT and p(g2T-TT). These two values are consistent, and hence, we interpret this as an indication that the polymers adopt an overall planar geometry also in the locally ordered crystallites of 3D thin films. Such a small distance is only compatible with a certain degree of interdigitation of the side-chains. We can see this directly in the STM images, but a signature of this is also present in the GIWAXS data, particularly in the (001) d-spacing of pgBTTT, which is compatible with the expected spacing between antiparallel crystalline oligoethylene glycol helices.

OECTs. Incorporating pgBTTT as the channel material in organic electrochemical transistors (OECTs) produces high performing accumulation mode devices, the results of which are summarized in Table 3. OECTs with channel depth (d) of 108 ± 1 nm and a channel aspect ratio (W/L) of 10, display threshold voltages (V_t) of −242.9 ± 4.9 mV, with ON currents reaching ∼4 mA at a gate voltage (V_g) of −600 mV, and ON/OFF ratios of ∼10^5, Figures 6a,b and S10. This large modulation of channel current over a small voltage range leads to an exceptional gate transconductance (g_m) which captures a device's ability to amplify an input ($g_m = \partial I_d/\partial V_g$) and, in the case of pgBTTT devices, exceeds 20 mS at V_g = −0.6 V. In the saturation regime, g_m depends on device dimensions (d and W/L), V_t, and applied V_g following the relation:

$$g_m = \frac{Wd}{L}\mu C^*(V_t - V_g)$$

Thus, g_m is a device property and g_m values for different materials are not necessarily directly comparable. However, the mobility−capacitance product (μC^*) represents a universally comparable material figure of merit for organic mixed ionic-electronic conductors.[37] Given the device dimensions and V_t, a μC^* of 502 ± 18 F cm^{-1} V^{-1} s^{-1} was calculated. Alternatively, calculating this figure of merit from the C^* as determined by electrochemical impedance spectroscopy (EIS) and the saturation mobility (μ_{sat}) extracted from the slope of $I_d^{1/2}$ vs V_g plots, yields a value of 563 ± 33 F cm^{-1} V^{-1} s^{-1}, confirming this extremely high figure of merit. Investigating the constitutive elements of μC^* reveals that the main source of this large μC^* for pgBTTT was μ. The pgBTTT C^* was not especially high (164 ± 7 F cm^{-3}) while the μ_{sat} was quite large (3.44 ± 0.13 cm^2 V^{-1} s^{-1}). The pgBTTT $I_d^{1/2}$ vs V_g plots displays linear behavior with no kinks, Figure S10, indicating ideal saturation and a high confidence in the extracted μ_{sat} values.[53−55] These results were reproducible, with ideal

https://doi.org/10.1021/jacs.1c03516
J. Am. Chem. Soc. 2021, 143, 11007−11018

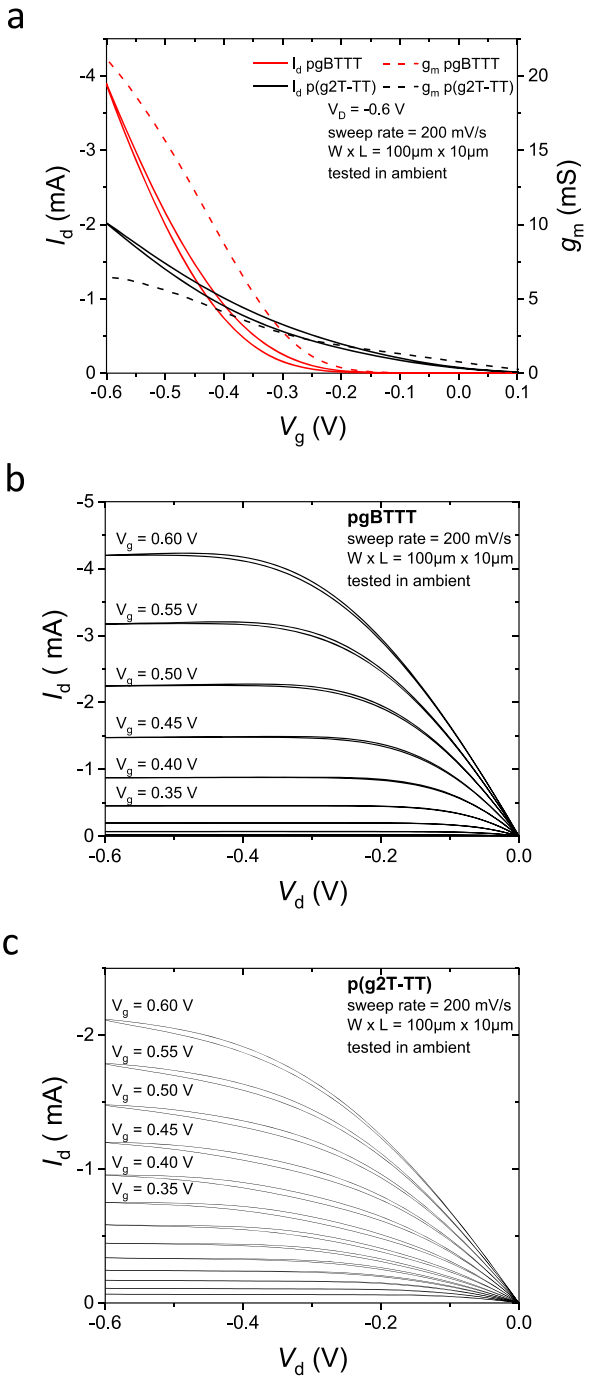

Figure 6. OECT performance: (a) Transfer curves (I_d vs V_g) and voltage dependent transconductance (g_m) of representative pgBTTT and p(g2T-TT) devices, and output curves (I_d vs V_d) of the same (b) pgBTTT and (c) p(g2T-TT) devices.

saturation, V_t, g_m, extracted μ_{sat}, and record high μC^* consistent across all devices tested, reflected in the low uncertainties in Table 3 and the raw $I-V$ curves in Figure S10.

A p(g2T-TT)-based OECT fabricated in an identical manner, with identical W/L, similar channel depth and comparable molecular weight, gave a mobility, capacitance, and μC^* figure of merit of 0.41 ± 0.14 $cm^2\ V^{-1}\ s^{-1}$, 244 ± 51 F cm^{-3}, and 90 ± 6 F $cm^{-1}\ V^{-1}\ s^{-1}$, respectively. Comparing the two materials (Figure 6 and Table 3), the pgBTTT μ_{sat} was over eight times greater than that of p(g2T-TT); pgBTTT's C^* was one-third less than that of p(g2T-TT), and pgBTTT μC^* represented a 6-fold improvement over that of p(g2T-TT). In addition to the improved μ_{sat} and μC^* figure of merit, the negative shifted V_t of pgBTTT OECTs (due to a combination of larger IP and shallower subthreshold slope) was an added benefit as the low V_t of p(g2T-TT) undermines the stability of the device's OFF state.[32]

Electrochemical Quartz Crystal Microbalance with Dissipation of Energy (eQCM-D) Measurements. Polymer solutions were cast directly on the eQCM-D sensors. The resultant thin film thicknesses in both air and NaCl (aq.) 0.1 M were calculated, as described in detail in the Experimental Section and Figure S18. The sensors in air were exposed to NaCl (aq.) 0.1 M, and the QCM-D signals (frequency and dissipation shifts) stabilized, indicating that the system was in equilibrium, and no more ion exchange was taking place between the electrolyte and the polymer. pgBTTT was found to swell 16% when immersed in NaCl (aq.) 0.1 M, similar to p(g2T-TT)'s swelling of 12%, in line with our previously published study.[17] After the passive swelling measurements, we applied a doping potential at 0.5 V vs Ag/AgCl for 60 s in the case of both polymers while monitoring the changes in QCM-D signals. Figure 7 shows a shift in frequency and dissipation, suggesting that both polymers exhibit significant mass uptake when charged at 0.5 V. We found that pgBTTT increased its mass by 3290 ng (46 wt % swelling) while p(g2T-TT) mass' increased by 3695 ng (65 wt % swelling) due to ions and water drifting in the polymer during doping. Simultaneously, we recorded the current produced by each polymer film (Figure S19). Using the current−time and mass-time profiles, we calculated the number of charges injected into the films (i.e., the volumetric capacitance), as well as the water density loaded in the polymer film.[17] The charge density calculated by integrating the current vs time curves (Figure S19) was 4.58 × 10^{-4} and 7.72 × 10^{-4} C/cm^2 for pgBTTT and p(g2T-TT), respectively. These values correspond to 141 and 266 F cm^{-3} for pgBTTT and p(g2T-TT), respectively, in line with the values calculated from EIS measurements. By correlating the mass uptake to the charge loaded in the films, we found the water density within the polymer films upon doping to be 2.05 × 10^{22} and 2.85 × 10^{22} H_2O molecules/cm^3 for pgBTTT and p(g2T-TT), respectively. These numbers suggest that both polymers take up water during charging, while the active hydration of p(g2T-TT) is higher. p(g2T-TT) also exhibits substantial dissipation shifts and their distribution among different overtones compared to pgBTTT (Figure 7 middle row). These results suggest that the pgBTTT film is more rigid during charging compared to p(g2T-TT), most possibly because of the lower water uptake during charging. We have previously shown an inverse relation between the hole mobility and water uptake in polymer mixed conductors with EG side chains.[17,56] The lower water density accumulating in pgBTTT during doping can help the polymer maintain a more rigid structure, minimizing molecular packing disruption, and maintaining higher hole mobility.

CONCLUSION

We have synthesized the glycol chain analogue of pBTTT and evaluated its molecular conformation, thin film morphology, and performance in an organic electrochemical transistor. The polymer combines the backbone planarity, intermolecular assembly and charge carrier transport properties of pBTTT with the bulk ion doping ability of p(g2T-TT). We have demonstrated that regiochemistry plays an important role in

https://doi.org/10.1021/jacs.1c03516
J. Am. Chem. Soc. 2021, 143, 11007−11018

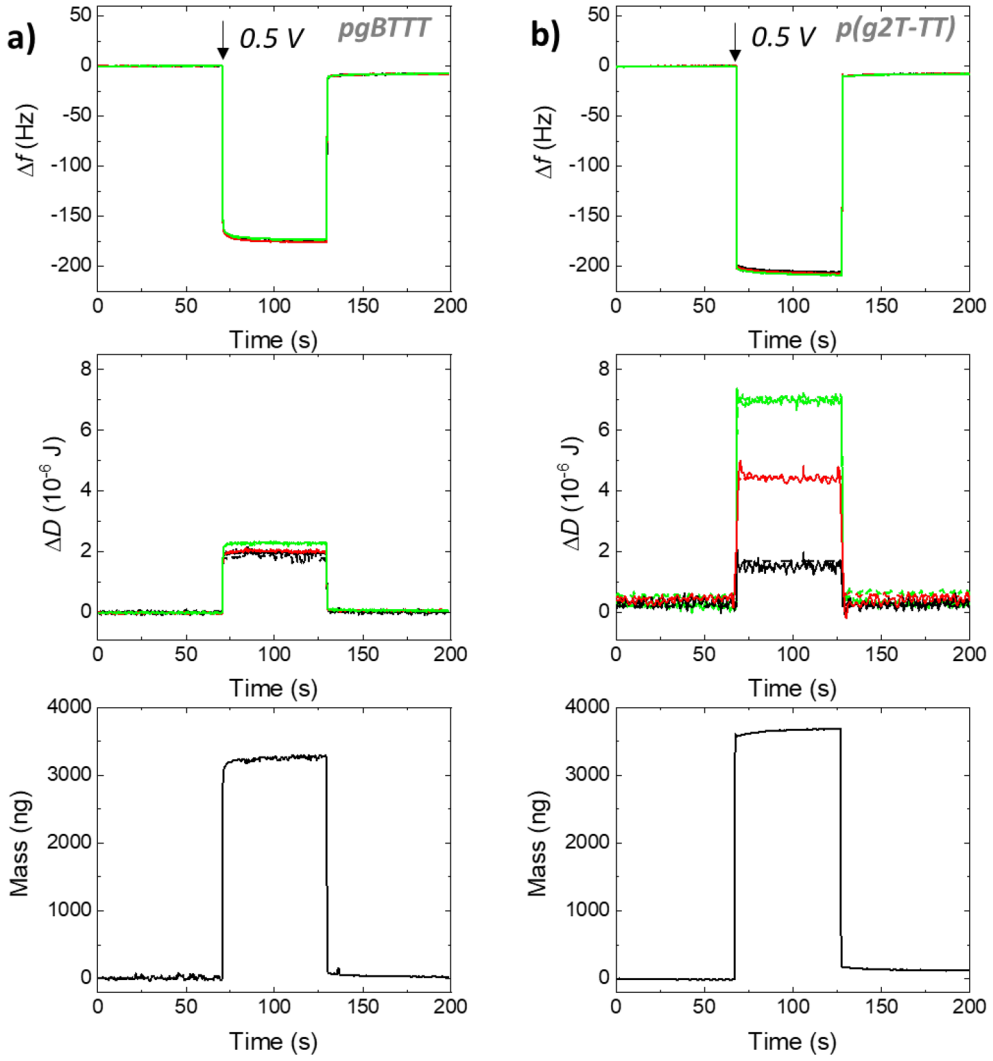

Figure 7. Frequency shifts (Δf, top row), dissipation of energy (ΔD, middle row), and calculated mass shifts for (a) pgBTTT and (b) p(g2T-TT) polymer films cast on Au-coated sensors, recorded in NaCl (aq.) 0.1 M when a 60 s doping pulse at V = 0.5 V vs V_{OC} is applied. The overtones shown and chosen for the analysis are the 3rd, 5th and 7th, in black, red, and green solid lines, respectively.

not only the polymer conformation, but its subsequent self-assembly, thin film morphology, and electronic properties. DFT calculations were performed to explain the improved planarity of the pgBTTT polymer, arising from spreading the S−O planarizing interactions across a wider section of the polymer. The polymer microstructure change was confirmed using GIWAXS, with pgBTTT showing a higher ordered fraction, with beam scattering being five times more intense than that of p(g2T-TT). The presence of significant in- and out-of-plane π-stacking in pgBTTT (versus mostly in-plane π-stacking in p(g2T-TT)) likely improves the three-dimensional percolation necessary for electronic charge transport. STM measurements showed that the intermolecular interactions of both pgBTTT and p(g2T-TT) are stabilized by interdigitation of their triethylene glycol side chains. Moreover, the excellent agreement between the measured 2D molecular separation and the GIWAXS-determined lamellar spacing, suggests an overall planar geometry of the polymers in the crystalline regions of the 3D thin films. eQCM-D measurements indicated a similar water uptake for pgBTTT and p(g2T-TT), 16% and 12%, respectively, in the absence of a voltage (passive swelling). However, at 0.5 V, pgBTTT water uptake was less than that of p(g2T-TT) with swelling of 46 wt % for pgBTTT compared to 65 wt % for p(g2T-TT). As a result, pgBTTT maintains a more rigid structure during doping, minimizing molecular packing disruption and therefore maintaining higher hole mobility. The figure of merit used to evaluate channel materials in OECT devices, namely the mobility−capacitance product (μC^*) of pgBTTT, was 502 ± 18 F cm^{-1} V^{-1} s^{-1}, a consequence of its high mobility (μ_{sat}) of 3.44 ± 0.13 cm^2 V^{-1} s^{-1}.

■ ASSOCIATED CONTENT

Supporting Information

The Supporting Information is available free of charge at https://pubs.acs.org/doi/10.1021/jacs.1c03516.

Synthesis of pgBTTT, ^{1}H and ^{13}C{^{1}H} NMR spectra, GC-MS and HR-MS measurements, DFT calculations (variation in dihedral angle, torsional potential energy surface, Hirshfeld charge distribution), TGA and DSC traces, OECT devices and EIS measurements, GIWAXS line cuts, spectroelectrochemistry, cyclic voltammetry, and eQCM-D measurements, including Figures S1−S20 (PDF)

https://doi.org/10.1021/jacs.1c03516
J. Am. Chem. Soc. 2021, 143, 11007−11018

AUTHOR INFORMATION

Corresponding Author

Iain McCulloch − *Physical Science and Engineering Division, King Abdullah University of Science and Technology (KAUST), Thuwal 23955-6900, Saudi Arabia; Department of Chemistry, Chemistry Research Laboratory, University of Oxford, Oxford OX1 3TA, U.K.;* orcid.org/0000-0002-6340-7217; Email: iain.mcculloch@chem.ox.ac.uk

Authors

Rawad K. Hallani − *Physical Science and Engineering Division, King Abdullah University of Science and Technology (KAUST), Thuwal 23955-6900, Saudi Arabia;* orcid.org/0000-0002-9561-750X

Bryan D. Paulsen − *Department of Biomedical Engineering, Northwestern University, Evanston, Illinois 60208, United States;* orcid.org/0000-0002-0923-8475

Anthony J. Petty II − *Department of Biomedical Engineering, Northwestern University, Evanston, Illinois 60208, United States;* orcid.org/0000-0002-5831-0314

Rajendar Sheelamanthula − *Physical Science and Engineering Division, King Abdullah University of Science and Technology (KAUST), Thuwal 23955-6900, Saudi Arabia*

Maximilian Moser − *Department of Chemistry, Chemistry Research Laboratory, University of Oxford, Oxford OX1 3TA, U.K.;* orcid.org/0000-0002-3293-9309

Karl J. Thorley − *Department of Chemistry, University of Kentucky, Lexington, Kentucky 40506, United States;* orcid.org/0000-0003-0665-3363

Wonil Sohn − *Department of Biomedical Engineering, Northwestern University, Evanston, Illinois 60208, United States;* orcid.org/0000-0001-5591-6639

Reem B. Rashid − *Department of Biomedical Engineering, Northwestern University, Evanston, Illinois 60208, United States;* orcid.org/0000-0001-9503-3881

Achilleas Savva − *Organic Bioelectronics Laboratory, Biological and Environmental Science and Engineering, King Abdullah University of Science and Technology (KAUST), Thuwal 23955-6900, Saudi Arabia;* orcid.org/0000-0002-0197-0290

Stefania Moro − *Department of Chemistry, University of Warwick, Coventry CV4 7AL, U.K.;* orcid.org/0000-0001-8445-4509

Joseph P. Parker − *Department of Chemistry, University of Warwick, Coventry CV4 7AL, U.K.;* orcid.org/0000-0002-2601-8482

Oscar Drury − *Department of Chemistry, University of Warwick, Coventry CV4 7AL, U.K.;* orcid.org/0000-0003-0583-930X

Maryam Alsufyani − *Physical Science and Engineering Division, King Abdullah University of Science and Technology (KAUST), Thuwal 23955-6900, Saudi Arabia;* orcid.org/0000-0003-4097-7900

Marios Neophytou − *Physical Science and Engineering Division, King Abdullah University of Science and Technology (KAUST), Thuwal 23955-6900, Saudi Arabia;* orcid.org/0000-0003-2207-4193

Jan Kosco − *Physical Science and Engineering Division, King Abdullah University of Science and Technology (KAUST), Thuwal 23955-6900, Saudi Arabia;* orcid.org/0000-0002-1054-9131

Sahika Inal − *Organic Bioelectronics Laboratory, Biological and Environmental Science and Engineering, King Abdullah University of Science and Technology (KAUST), Thuwal 23955-6900, Saudi Arabia;* orcid.org/0000-0002-1166-1512

Giovanni Costantini − *Department of Chemistry, University of Warwick, Coventry CV4 7AL, U.K.;* orcid.org/0000-0001-7916-3440

Jonathan Rivnay − *Department of Biomedical Engineering, Northwestern University, Evanston, Illinois 60208, United States; Simpson Querrey Institute, Northwestern University, Chicago, Illinois 60611, United States;* orcid.org/0000-0002-0602-6485

Complete contact information is available at: https://pubs.acs.org/10.1021/jacs.1c03516

Notes

The authors declare no competing financial interest.

ACKNOWLEDGMENTS

The research reported in this publication was supported by funding from King Abdullah University of Science and Technology (KAUST), including Office of Sponsored Research (OSR) awards no. OSR-2018-CRG/CCF-3079, OSR-2019-CRG8-4086 and OSR-2018-CRG7-3749. We acknowledge funding from ERC Synergy Grant SC2 (610115), the European Union's Horizon 2020 research and innovation programme under grant agreement no. 952911, project BOOSTER and grant agreement no. 862474, project RoLA-FLEX, as well as EPSRC Project EP/T026219/1. B.D.P. and J.R. gratefully acknowledge support from the National Science Foundation grant no. NSF DMR-1751308. W.S. gratefully acknowledges support from the Northwestern University Office of Undergraduate Research. Special thanks to Joseph Strzalka and Qingteng Zhang for beamline assistance. This research used resources of the Advanced Photon Source, a U.S. Department of Energy (DOE) Office of Science User Facility operated for the DOE Office of Science by Argonne National Laboratory under Contract No. DE-AC02-06CH11357. This work utilized Keck-II facility of Northwestern University's NUANCE Center and Northwestern University Micro/Nano Fabrication Facility (NUFAB), which are both partially supported by Soft and Hybrid Nanotechnology Experimental (SHyNE) Resource (NSF ECCS-1542205), the Materials Research Science and Engineering Center (NSF DMR-1720139), the State of Illinois, and Northwestern University. Additionally, the Keck-II facility is partially supported by the International Institute for Nanotechnology (IIN); the Keck Foundation; and the State of Illinois, through the IIN. S.M. acknowledges funding though an EU Chancellor's Scholarship by the University of Warwick. J.P.P. acknowledges support by the Biotechnology and Biological Sciences Research Council (BBSRC) and University of Warwick funded Midlands Integrative Biosciences Training Partnership (MIBTP) (grant number BB/M01116X/1).

REFERENCES

(1) Song, E.; Li, J.; Won, S. M.; Bai, W.; Rogers, J. A. Materials for flexible bioelectronic systems as chronic neural interfaces. *Nat. Mater.* **2020**, *19* (6), 590−603.

(2) Isaksson, J.; Kjäll, P.; Nilsson, D.; Robinson, N.; Berggren, M.; Richter-Dahlfors, A. Electronic control of Ca 2+ signalling in neuronal cells using an organic electronic ion pump. *Nat. Mater.* **2007**, *6* (9), 673−679.

(3) Arbring Sjöström, T.; Berggren, M.; Gabrielsson, E. O.; Janson, P.; Poxson, D. J.; Seitanidou, M.; Simon, D. T. A decade of iontronic delivery devices. *Advanced Materials Technologies* **2018**, *3* (5), 1700360.
(4) Garcia-Cordero, E.; Bellando, F.; Zhang, J.; Wildhaber, F.; Longo, J.; Guérin, H.; Ionescu, A. M. Three-Dimensional Integrated Ultra-Low-Volume Passive Microfluidics with Ion-Sensitive Field-Effect Transistors for Multiparameter Wearable Sweat Analyzers. *ACS Nano* **2018**, *12* (12), 12646−12656.
(5) Yu, Y.; Nyein, H. Y. Y.; Gao, W.; Javey, A. Flexible Electrochemical Bioelectronics: The Rise of In Situ Bioanalysis. *Adv. Mater.* **2020**, *32* (15), 1902083.
(6) Ohayon, D.; Nikiforidis, G.; Savva, A.; Giugni, A.; Wustoni, S.; Palanisamy, T.; Chen, X.; Maria, I. P.; Di Fabrizio, E.; Costa, P. M. F. J.; McCulloch, I.; Inal, S. Biofuel powered glucose detection in bodily fluids with an n-type conjugated polymer. *Nat. Mater.* **2020**, *19* (4), 456−463.
(7) Wustoni, S.; Combe, C.; Ohayon, D.; Akhtar, M. H.; McCulloch, I.; Inal, S. Membrane-Free Detection of Metal Cations with an Organic Electrochemical Transistor. *Adv. Funct. Mater.* **2019**, *29* (44), 1904403.
(8) Kawan, M.; Hidalgo, T. C.; Du, W.; Pappa, A.-M.; Owens, R. M.; McCulloch, I.; Inal, S. Monitoring supported lipid bilayers with n-type organic electrochemical transistors. *Mater. Horiz.* **2020**, *7* (9), 2348−2358.
(9) Paulsen, B. D.; Tybrandt, K.; Stavrinidou, E.; Rivnay, J. Organic mixed ionic−electronic conductors. *Nat. Mater.* **2020**, *19* (1), 13−26.
(10) Bernards, D. A.; Malliaras, G. G. Steady-state and transient behavior of organic electrochemical transistors. *Adv. Funct. Mater.* **2007**, *17* (17), 3538−3544.
(11) Rivnay, J.; Owens, R. M.; Malliaras, G. G. The Rise of Organic Bioelectronics. *Chem. Mater.* **2014**, *26* (1), 679−685.
(12) Fratini, S.; Nikolka, M.; Salleo, A.; Schweicher, G.; Sirringhaus, H. Charge transport in high-mobility conjugated polymers and molecular semiconductors. *Nat. Mater.* **2020**, *19* (5), 491−502.
(13) Prins, P.; Grozema, F. C.; Schins, J. M.; Patil, S.; Scherf, U.; Siebbeles, L. D. A. High Intrachain Hole Mobility on Molecular Wires of Ladder-Type Poly(p-Phenylenes). *Phys. Rev. Lett.* **2006**, *96* (14), 146601.
(14) Rivnay, J.; Inal, S.; Salleo, A.; Owens, R. M.; Berggren, M.; Malliaras, G. G. Organic electrochemical transistors. *Nature Reviews Materials* **2018**, *3* (2), 17086.
(15) Said, E.; Robinson, N. D.; Nilsson, D.; Svensson, P.-O.; Berggren, M. Visualizing the electric field in electrolytes using electrochromism from a conjugated polymer. *Electrochem. Solid-State Lett.* **2005**, *8* (2), H12.
(16) Flagg, L. Q.; Bischak, C. G.; Onorato, J. W.; Rashid, R. B.; Luscombe, C. K.; Ginger, D. S. Polymer Crystallinity Controls Water Uptake in Glycol Side-Chain Polymer Organic Electrochemical Transistors. *J. Am. Chem. Soc.* **2019**, *141* (10), 4345−4354.
(17) Savva, A.; Hallani, R.; Cendra, C.; Surgailis, J.; Hidalgo, T. C.; Wustoni, S.; Sheelamanthula, R.; Chen, X.; Kirkus, M.; Giovannitti, A.; Salleo, A.; McCulloch, I.; Inal, S. Balancing Ionic and Electronic Conduction for High-Performance Organic Electrochemical Transistors. *Adv. Funct. Mater.* **2020**, *30* (11), 1907657.
(18) Wang, Y.; Zhu, C.; Pfattner, R.; Yan, H.; Jin, L.; Chen, S.; Molina-Lopez, F.; Lissel, F.; Liu, J.; Rabiah, N. I.; et al. A highly stretchable, transparent, and conductive polymer. *Science advances* **2017**, *3* (3), e1602076.
(19) Kim, S.-M.; Kim, C.-H.; Kim, Y.; Kim, N.; Lee, W.-J.; Lee, E.-H.; Kim, D.; Park, S.; Lee, K.; Rivnay, J.; Yoon, M.-H. Influence of PEDOT:PSS crystallinity and composition on electrochemical transistor performance and long-term stability. *Nat. Commun.* **2018**, *9* (1), 3858.
(20) Gueye, M. N.; Carella, A.; Faure-Vincent, J.; Demadrille, R.; Simonato, J.-P. Progress in understanding structure and transport properties of PEDOT-based materials: A critical review. *Prog. Mater. Sci.* **2020**, *108*, 100616.
(21) Proctor, C. M.; Rivnay, J.; Malliaras, G. G. Understanding volumetric capacitance in conducting polymers. *J. Polym. Sci., Part B: Polym. Phys.* **2016**, *54* (15), 1433−1436.
(22) Shi, H.; Liu, C.; Jiang, Q.; Xu, J. Effective approaches to improve the electrical conductivity of PEDOT:PSS: a review. *Advanced Electronic Materials* **2015**, *1* (4), 1500017.
(23) Giovannitti, A.; Sbircea, D.-T.; Inal, S.; Nielsen, C. B.; Bandiello, E.; Hanifi, D. A.; Sessolo, M.; Malliaras, G. G.; McCulloch, I.; Rivnay, J. Controlling the mode of operation of organic transistors through side-chain engineering. *Proc. Natl. Acad. Sci. U. S. A.* **2016**, *113* (43), 12017−12022.
(24) Giovannitti, A.; Nielsen, C. B.; Sbircea, D.-T.; Inal, S.; Donahue, M.; Niazi, M. R.; Hanifi, D. A.; Amassian, A.; Malliaras, G. G.; Rivnay, J.; McCulloch, I. N-type organic electrochemical transistors with stability in water. *Nat. Commun.* **2016**, *7* (1), 13066.
(25) Zeglio, E.; Inganäs, O. Active Materials for Organic Electrochemical Transistors. *Adv. Mater.* **2018**, *30* (44), 1800941.
(26) Moser, M.; Ponder, J. F., Jr.; Wadsworth, A.; Giovannitti, A.; McCulloch, I. Materials in Organic Electrochemical Transistors for Bioelectronic Applications: Past, Present, and Future. *Adv. Funct. Mater.* **2019**, *29* (21), 1807033.
(27) Moser, M.; Hidalgo, T. C.; Surgailis, J.; Gladisch, J.; Ghosh, S.; Sheelamanthula, R.; Thiburce, Q.; Giovannitti, A.; Salleo, A.; Gasparini, N.; Wadsworth, A.; Zozoulenko, I.; Berggren, M.; Stavrinidou, E.; Inal, S.; McCulloch, I. Side Chain Redistribution as a Strategy to Boost Organic Electrochemical Transistor Performance and Stability. *Adv. Mater.* **2020**, *32* (37), 2002748.
(28) Nielsen, C. B.; Giovannitti, A.; Sbircea, D.-T.; Bandiello, E.; Niazi, M. R.; Hanifi, D. A.; Sessolo, M.; Amassian, A.; Malliaras, G. G.; Rivnay, J.; McCulloch, I. Molecular Design of Semiconducting Polymers for High-Performance Organic Electrochemical Transistors. *J. Am. Chem. Soc.* **2016**, *138* (32), 10252−10259.
(29) Åsberg, P.; Nilsson, K. P. R.; Inganäs, O. Surface energy modified chips for detection of conformational states and enzymatic activity in biomolecules. *Langmuir* **2006**, *22* (5), 2205−2211.
(30) Savagian, L. R.; Österholm, A. M.; Ponder, J. F., Jr.; Barth, K. J.; Rivnay, J.; Reynolds, J. R. Balancing Charge Storage and Mobility in an Oligo(Ether) Functionalized Dioxythiophene Copolymer for Organic- and Aqueous- Based Electrochemical Devices and Transistors. *Adv. Mater.* **2018**, *30* (50), 1804647.
(31) Schmode, P.; Ohayon, D.; Reichstein, P. M.; Savva, A.; Inal, S.; Thelakkat, M. High-Performance Organic Electrochemical Transistors Based on Conjugated Polyelectrolyte Copolymers. *Chem. Mater.* **2019**, *31* (14), 5286−5295.
(32) Giovannitti, A.; Rashid, R. B.; Thiburce, Q.; Paulsen, B. D.; Cendra, C.; Thorley, K.; Moia, D.; Mefford, J. T.; Hanifi, D.; Weiyuan, D.; Moser, M.; Salleo, A.; Nelson, J.; McCulloch, I.; Rivnay, J. Energetic Control of Redox-Active Polymers toward Safe Organic Bioelectronic Materials. *Adv. Mater.* **2020**, *32* (16), 1908047.
(33) Wang, Y.; Zeglio, E.; Liao, H.; Xu, J.; Liu, F.; Li, Z.; Maria, I. P.; Mawad, D.; Herland, A.; McCulloch, I.; Yue, W. Hybrid Alkyl−Ethylene Glycol Side Chains Enhance Substrate Adhesion and Operational Stability in Accumulation Mode Organic Electrochemical Transistors. *Chem. Mater.* **2019**, *31* (23), 9797−9806.
(34) Moser, M.; Savva, A.; Thorley, K.; Paulsen, B. D.; Hidalgo, T. C.; Ohayon, D.; Chen, H.; Giovannitti, A.; Marks, A.; Gasparini, N.; Wadsworth, A.; Rivnay, J.; Inal, S.; McCulloch, I. Polaron Delocalization in Donor−Acceptor Polymers and its Impact on Organic Electrochemical Transistor Performance. *Angew. Chem., Int. Ed.* **2021**, *60* (14), 7777−7785.
(35) Giovannitti, A.; Maria, I. P.; Hanifi, D.; Donahue, M. J.; Bryant, D.; Barth, K. J.; Makdah, B. E.; Savva, A.; Moia, D.; Zetek, M.; Barnes, P. R. F.; Reid, O. G.; Inal, S.; Rumbles, G.; Malliaras, G. G.; Nelson, J.; Rivnay, J.; McCulloch, I. The Role of the Side Chain on the Performance of N-type Conjugated Polymers in Aqueous Electrolytes. *Chem. Mater.* **2018**, *30* (9), 2945−2953.
(36) Moser, M.; Savagian, L. R.; Savva, A.; Matta, M.; Ponder, J. F.; Hidalgo, T. C.; Ohayon, D.; Hallani, R.; Reisjalali, M.; Troisi, A.; Wadsworth, A.; Reynolds, J. R.; Inal, S.; McCulloch, I. Ethylene

https://doi.org/10.1021/jacs.1c03516
J. Am. Chem. Soc. 2021, 143, 11007−11018

Glycol-Based Side Chain Length Engineering in Polythiophenes and its Impact on Organic Electrochemical Transistor Performance. *Chem. Mater.* **2020**, *32* (15), 6618−6628.
(37) Inal, S.; Malliaras, G. G.; Rivnay, J. Benchmarking organic mixed conductors for transistors. *Nat. Commun.* **2017**, *8* (1), 1767.
(38) Hallani, R. K.; Thorley, K. J.; Mei, Y.; Parkin, S. R.; Jurchescu, O. D.; Anthony, J. E. Structural and Electronic Properties of Crystalline, Isomerically Pure Anthradithiophene Derivatives. *Adv. Funct. Mater.* **2016**, *26* (14), 2341−2348.
(39) Takahashi, M.; Masui, K.; Sekiguchi, H.; Kobayashi, N.; Mori, A.; Funahashi, M.; Tamaoki, N. Palladium-Catalyzed C−H Homocoupling of Bromothiophene Derivatives and Synthetic Application to Well-Defined Oligothiophenes. *J. Am. Chem. Soc.* **2006**, *128* (33), 10930−10933.
(40) Chabinyc, M. L.; Toney, M. F.; Kline, R. J.; McCulloch, I.; Heeney, M. X-ray Scattering Study of Thin Films of Poly(2,5-bis(3-alkylthiophen-2-yl)thieno[3,2-b]thiophene). *J. Am. Chem. Soc.* **2007**, *129* (11), 3226−3237.
(41) McCulloch, I.; Heeney, M.; Bailey, C.; Genevicius, K.; MacDonald, I.; Shkunov, M.; Sparrowe, D.; Tierney, S.; Wagner, R.; Zhang, W.; Chabinyc, M. L.; Kline, R. J.; McGehee, M. D.; Toney, M. F. Liquid-crystalline semiconducting polymers with high charge-carrier mobility. *Nat. Mater.* **2006**, *5* (4), 328−333.
(42) French, A. C.; Thompson, A. L.; Davis, B. G. High-Purity Discrete PEG-Oligomer Crystals Allow Structural Insight. *Angew. Chem., Int. Ed.* **2009**, *48* (7), 1248−1252.
(43) Brinkmann, M.; Gonthier, E.; Bogen, S.; Tremel, K.; Ludwigs, S.; Hufnagel, M.; Sommer, M. Segregated versus Mixed Interchain Stacking in Highly Oriented Films of Naphthalene Diimide Bithiophene Copolymers. *ACS Nano* **2012**, *6* (11), 10319−10326.
(44) Ohayon, D.; Savva, A.; Du, W.; Paulsen, B. D.; Uguz, I.; Ashraf, R. S.; Rivnay, J.; McCulloch, I.; Inal, S. Influence of Side Chains on the n-Type Organic Electrochemical Transistor Performance. *ACS Appl. Mater. Interfaces* **2021**, *13* (3), 4253−4266.
(45) Maria, I. P.; Paulsen, B. D.; Savva, A.; Ohayon, D.; Wu, R.; Hallani, R.; Basu, A.; Du, W.; Anthopoulos, T. D.; Inal, S.; Rivnay, J.; McCulloch, I.; Giovannitti, A. The Effect of Alkyl Spacers on the Mixed Ionic-Electronic Conduction Properties of N-Type Polymers. *Adv. Funct. Mater.* **2021**, *31* (14), 2008718.
(46) Warr, D. A.; Perdigão, L. M. A.; Pinfold, H.; Blohm, J.; Stringer, D.; Leventis, A.; Bronstein, H.; Troisi, A.; Costantini, G. Sequencing conjugated polymers by eye. *Science Advances* **2018**, *4* (6), eaas9543.
(47) Chen, H.; Wadsworth, A.; Ma, C.; Nanni, A.; Zhang, W.; Nikolka, M.; Luci, A. M. T.; Perdigão, L. M. A.; Thorley, K. J.; Cendra, C.; Larson, B.; Rumbles, G.; Anthopoulos, T. D.; Salleo, A.; Costantini, G.; Sirringhaus, H.; McCulloch, I. The Effect of Ring Expansion in Thienobenzo[b]indacenodithiophene Polymers for Organic Field-Effect Transistors. *J. Am. Chem. Soc.* **2019**, *141* (47), 18806−18813.
(48) Lawton, S. S.; Warr, D.; Perdigão, L. M. A.; Chang, Y.; Pron, A.; Costantini, G.; Haddleton, D. M. Determining the sequence and backbone structure of "semi-statistical" copolymers as donor−acceptor polymers in organic solar cells. *Sustainable Energy & Fuels* **2020**, *4* (4), 2026−2034.
(49) Xiao, M.; Kang, B.; Lee, S. B.; Perdigão, L. M. A.; Luci, A.; Warr, D. A.; Senanayak, S. P.; Nikolka, M.; Statz, M.; Wu, Y.; Sadhanala, A.; Schott, S.; Carey, R.; Wang, Q.; Lee, M.; Kim, C.; Onwubiko, A.; Jellett, C.; Liao, H.; Yue, W.; Cho, K.; Costantini, G.; McCulloch, I.; Sirringhaus, H. Anisotropy of Charge Transport in a Uniaxially Aligned Fused Electron-Deficient Polymer Processed by Solution Shear Coating. *Adv. Mater.* **2020**, *32* (23), 2000063.
(50) Keg, P.; Lohani, A.; Fichou, D.; Lam, Y. M.; Wu, Y.; Ong, B. S.; Mhaisalkar, S. G. Direct Observation of Alkyl Chain Interdigitation in Conjugated Polyquarterthiophene Self-Organized on Graphite Surfaces. *Macromol. Rapid Commun.* **2008**, *29* (14), 1197−1202.
(51) McKeown, G. R.; Fang, Y.; Obhi, N. K.; Manion, J. G.; Perepichka, D. F.; Seferos, D. S. Synthesis of Macrocyclic Poly(3-hexylthiophene) and Poly(3-heptylselenophene) by Alkyne Homocoupling. *ACS Macro Lett.* **2016**, *5* (10), 1075−1079.
(52) Kline, R. J.; DeLongchamp, D. M.; Fischer, D. A.; Lin, E. K.; Richter, L. J.; Chabinyc, M. L.; Toney, M. F.; Heeney, M.; McCulloch, I. Critical Role of Side-Chain Attachment Density on the Order and Device Performance of Polythiophenes. *Macromolecules* **2007**, *40* (22), 7960−7965.
(53) Bittle, E. G.; Basham, J. I.; Jackson, T. N.; Jurchescu, O. D.; Gundlach, D. J. Mobility overestimation due to gated contacts in organic field-effect transistors. *Nat. Commun.* **2016**, *7* (1), 10908.
(54) Choi, H. H.; Cho, K.; Frisbie, C. D.; Sirringhaus, H.; Podzorov, V. Critical assessment of charge mobility extraction in FETs. *Nat. Mater.* **2018**, *17* (1), 2−7.
(55) Paterson, A. F.; Singh, S.; Fallon, K. J.; Hodsden, T.; Han, Y.; Schroeder, B. C.; Bronstein, H.; Heeney, M.; McCulloch, I.; Anthopoulos, T. D. Recent Progress in High-Mobility Organic Transistors: A Reality Check. *Adv. Mater.* **2018**, *30* (36), 1801079.
(56) Savva, A.; Cendra, C.; Giugni, A.; Torre, B.; Surgailis, J.; Ohayon, D.; Giovannitti, A.; McCulloch, I.; Di Fabrizio, E.; Salleo, A.; Rivnay, J.; Inal, S. Influence of Water on the Performance of Organic Electrochemical Transistors. *Chem. Mater.* **2019**, *31* (3), 927−937.

https://doi.org/10.1021/jacs.1c03516
J. Am. Chem. Soc. 2021, 143, 11007−11018